Selective-area crystalline growth enables simple efficient back-contacted silicon heterojunction solar cells

Andrea Tomasi[1]*, Bertrand Paviet-Salomon[2], Quentin Jeangros[1,3], Jan Haschke[1], Gabriel Christmann[2], Loris Barraud[2], Antoine Descoeudres[2], Johannes Peter Seif[1], Sylvain Nicolay[2], Matthieu Despeisse[2], Stefaan De Wolf[4,1], Christophe Ballif[1,2]

[1] École Polytechnique Fédérale de Lausanne (EPFL), Institute of microengineering (IMT), Photovoltaics and Thin Film Electronics Laboratory, Rue de la Maladière 71b, CH-2000 Neuchâtel, Switzerland
[2] Centre Suisse d'Électronique et de Microtechnique (CSEM), PV-Center, Rue Jaquet-Droz 1, CH-2002 Neuchâtel, Switzerland
[3] University of Basel, Department of Physics, Klingelbergstrasse 82, CH-4056 Basel, Switzerland
[4] King Abdullah University of Science and Technology (KAUST), KAUST Solar Center (KSC), Thuwal, 23955-6900, Saudi Arabia

*e-mail: andrea.tomasi@epfl.ch

For crystalline silicon (c-Si) solar cells, voltages close to the theoretical limit are nowadays readily achievable when using passivating contacts. Conversely, maximal current generation requires the integration of the electron and hole contacts at the back of the solar cell to liberate its front from any shadowing loss. Recently, the world-record efficiency for c-Si single-junction solar cells was achieved by merging these two approaches in a single device; however, the complexity of fabricating this class of devices raises concerns about their commercial potential. In this work, we demonstrate a new contacting method that substantially simplifies the architecture and fabrication process of back-contacted silicon solar cells. We exploit the surface-dependent growth of silicon thin films, deposited by plasma processes, to eliminate the patterning of one of the doped carrier-collecting layers. Using then only one alignment step for electrode definition, we fabricate a proof-of-concept 9-cm^2 "tunnel-IBC" solar cell with a certified conversion efficiency >22.5%.

In recent decades, the market of photovoltaics has been consistently growing and the yearly installed photovoltaic capacity has increased from 328 MW_{peak} in 2001 to 50 GW_{peak} in 2015. This resulted in 2016 in a cumulative capacity of 235 GW_{peak} [1], largely based on crystalline-silicon (c-Si) solar-cell technologies [2], and contributing to about 1.3% of the global electricity production [3]. To further increase this number, the cost-competitiveness of photovoltaics must surpass that of classic, non-renewable energy sources and one possible way to do so is to raise the conversion efficiency of industrial c-Si solar cells [4, 5].

High power conversion efficiencies require maximizing the solar cell's respective electrical parameters: open-circuit voltage (V_{oc}), fill-factor (FF) and short-circuit current densities (J_{sc}). For the V_{oc} and FF, this is possible by using so-called passivating contacts, employing silicon oxide or hydrogenated amorphous silicon (a-Si:H) thin films to minimize charge carrier recombination at the electrical contacts to the c-Si wafer, with demonstrated record efficiencies for two-side-contacted solar cells of 25% [6] and 25.1% [7], respectively. Maximum J_{sc} values can be achieved using a back-contacted architecture, eliminating metal electrode shadowing and minimizing optical reflection and absorption losses at the front. Small-sized back-contacted solar cells, based on diffused silicon homo-junctions, were realized at several research institutes [8-11], showing a best conversion efficiency up to 24.4% [12]. Industrially, the back-contacted architecture was pioneered by Sunpower, recently reporting on large-area devices with very high J_{sc} values and efficiencies surpassing 25% [13].

Considering these achievements, integrating passivating contacts in a back-contacted architecture is the obvious c-Si single-junction solar-cell design towards highest conversion

efficiencies. Such approach has increasingly been researched in both academia and industry over the last decade [14-21], resulting in the last few years in several record devices with efficiencies ≥25% [22-26]. Technologically, it is of note that all these outstanding results have been reached with passivating contacts that are either silicon-oxide-based [22] or fabricated by low-temperature depositions of hydrogenated silicon thin films [24-26], distinctive of the so-called silicon heterojunction (SHJ) technology [27]. Most recently in 2016, with a interdigitated back-contacted SHJ (IBC-SHJ) device, Kaneka achieved the impressive conversion efficiency of 26.6% [28], which is now approaching the theoretical limit for single-junction solar cells based on c-Si of 29.4% [29].

Whereas the high-efficiency potential of back-contacted devices based on the SHJ technology has been clearly shown, their fabrication with industry-relevant methods and low-complexity processing is still largely unresolved. The sole disclosed fabrication process of a top-efficiency (>25%) IBC-SHJ solar cell reveals the need for several wet-chemical etching or cleaning processes, as well as alignment and photolithographic patterning steps [25], making it unsuitable for low-cost, high-throughput manufacturing of solar cells.

In this article, we demonstrate a radically simplified self-aligned, bottom-up approach to interdigitated back-contact formation that exploits the surface-dependency of silicon thin-film growth obtained by plasma-enhanced chemical vapor deposition (PECVD). The local crystallinity of the deposited hydrogenated silicon (Si:H) material mimics that of the underlying film and, in this way, we can form a doped bilayer offering tailored heterogeneous conductivity properties. This enables an interdigitated back-contacted (IBC) device concept with drastically simplified

alignment requirements and fabrication. This solar cell is hereafter referred to as “tunnel-IBC”, because it relies on interband-tunneling electric transport [30] transversely across the deposited doped layers. Our best tunnel-IBC solar cell, realized with a single alignment step and no photolithographic patterning, has a conversion efficiency >22.5%, which improves slightly after light-soaking [31].

The tunnel-IBC solar cell

Fig. 1 shows the cross-sectional schematic of the tunnel-IBC solar cell, along with its low-complexity fabrication process. For comparison, the architecture of a conventional IBC-SHJ solar cell, as used by [24-26], is also shown in Fig. 1h. The distinctive element of the tunnel-IBC is the boron-doped p-type hydrogenated silicon [Si:H(p)] thin film which is deposited at the back side as a blanket layer, without patterning. Although similar approaches to IBC-SHJ simplification have been proposed [32, 33], their experimental feasibility remained unproven. Our tunnel-IBC solar cells use bifacially textured n-type c-Si [c-Si(n)] wafers, with front and back surfaces that are passivated by intrinsic hydrogenated amorphous silicon [a-Si:H(i)] interlayers of only a few nanometer in thickness.

At the front side, the thin a-Si:H(i) passivating film is then covered by a low-temperature (200 °C) silicon nitride (SiN_x) anti-reflection coating (ARC), providing excellent surface passivation, high transparency, and good light in-coupling. With this approach, front-side effective recombination velocities below 3 cm/s are obtainable, which is vital to achieve efficient minority-carrier collection in back-contacted devices [34, 35].

At the back side, we used an *in-situ* shadow mask during the PECVD deposition to pattern the phosphorous-doped n-type hydrogenated silicon [Si:H(n)] thin film, as shown in [36]. Following mask removal, a boron-doped p-type hydrogenated silicon [Si:H(p)] thin film is then deposited covering the entire back surface. In this way, without patterning, the hole collector is formed in those areas devoid of Si:H(n) where the Si:H(p) film is in direct contact with the a-Si:H(i) layer. Elsewhere, we have the electron collector consisting of an a-Si:H(i)/Si:H(n)/Si:H(p) triple layer

stack, which features an interband silicon tunnel junction (TJ) at the Si:H(n)/Si:H(p) interface. Notably, TJs are already successfully used in a variety of monolithic multi-junction solar cells [37-42], and in this new application we capitalize on this prior knowledge. The specific thin-film material requirements to achieve efficient interband-tunneling passivating contacts for electrons are discussed in details in the following section.

Key to this approach is the fact that the doped Si:H carrier collectors for electrons and holes are self-aligned with respect to each other. Thus, to finish the device, it is sufficient to subsequently align the interdigitated back electrodes to the pattern of the Si:H(n) thin film (which has the shape of a comb in our device). These electrodes were fabricated by depositing a transparent conductive oxide (TCO) film and a thicker metal overlayer, similar to the contacts used in two-side-contacted SHJ technology. These materials were then patterned with a simple and scalable process based on inkjet printing of an etch resist and wet-chemical etching as described elsewhere [36]. The total number of process steps to fabricate our device is remarkably low, ten when counting (1) c-Si wafer texturing , (2) front and (3) back a-Si:H(i) passivation, (4) front ARC, (5) back Si:H(n) and (6) Si:H(p) depositions, (7) TCO/metal deposition, (8) inkjet printing, (9) wet-chemical etching and (10) etch resist removal.

In addition to its low-complexity fabrication, our approach also tackles other critical limitations of back-contacted SHJ solar cells:

(i) For both interdigitated electrodes, the TCO film contacts exclusively the p-type Si:H thin-film material, which limits contact optimization to one specific interface.

Thus, the TCO film does not need to have different material properties in each contact, which would increase the complexity of the process.

(ii) In the tunnel-IBC design the deposited Si:H(p) layer has a uniform thickness. This eliminates the problem of insufficient charge-collecting film thickness along the perimeter of the contacts [43-46] that is associated with the tapered doped layer profiles produced by in-situ shadow-mask patterning [47, 48].

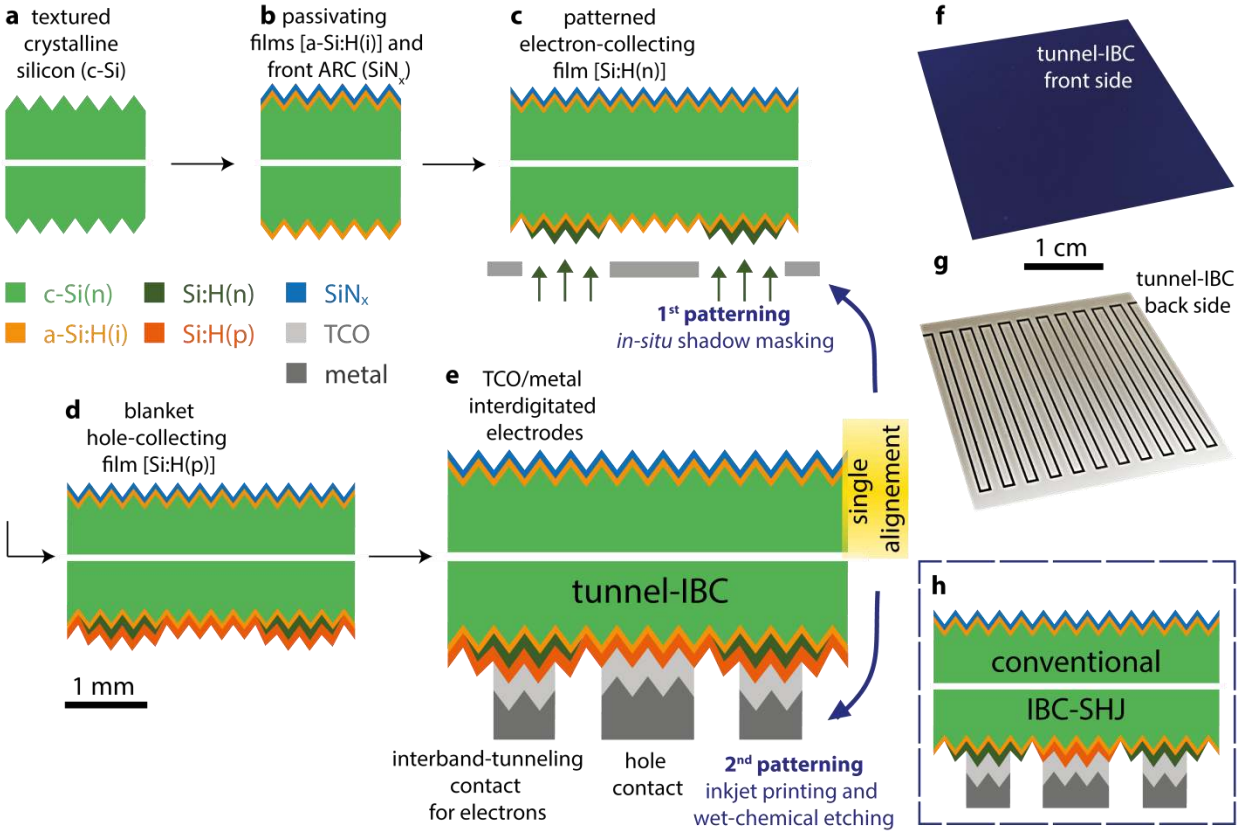

Fig. 1. The tunnel-IBC solar cell concept and its low-complexity fabrication process. Cross-sectional schematics of the tunnel-IBC solar cell showing the phases of its fabrication. **a,** Wafer wet-chemical texturing and cleaning. **b,** Wafer passivation with a-Si:H(i) films and SiN_x ARC deposition at the front. **c,** Patterned Si:H(n) film deposition via in-situ shadow masking. **d,** Full-area Si:H(p) film deposition. **e,** Full-area TCO/metal stack deposition and inkjet-patterning of the back electrodes. This last schematic reveals the special contacting scheme of the tunnel-IBC, including an efficient interband silicon TJ at the Si:H(n)/Si:H(p) interface. This approach makes patterning of the Si:H(p) film superfluous enabling a low-complexity fabrication process with only two photolithography-free patterning steps and a single alignment. **f**, Photograph of the front of the tunnel-IBC solar cell. **g,** Photograph of the back of the tunnel-IBC solar cell. **h**, Cross-sectional schematics of a conventional IBC-SHJ solar cell architecture, as used also in recent record devices [24-26]. For simplicity, the front stack is represented as a bilayer of a-Si:H(i) and

133 SiN_x, similarly as for the tunnel-IBC. We note that at the front alternative passivating films or a double ARC can also
134 be used.

Requirements for efficient tunnel-IBC solar cells and thin-film materials

Requirement I. In efficient tunnel-IBC solar cells, the interband-tunneling passivating contact for electrons (see close-up schematic in Fig. 2a) must collect and transport electrons from the c-Si absorber to the back electrode, without resistive losses. Hence, the first requirement is to integrate a low-resistance TJ at the interface of the p- and n-type Si:H thin films.

Requirement II. Our interband-tunneling contact must have good selectivity toward electrons, which also implies high passivation of the underlying c-Si surface. In passivating-contact technologies, carrier selectivity is obtained with an electric potential at the c-Si surface, induced by the carrier-collecting material [49, 50]. For a stack of sufficiently-thin layers, the resulting c-Si surface potential can be affected by the presence of overlying films that are not directly in contact with the c-Si surface. Even the uppermost film in thin three-layer stacks, such as the TCO film in SHJ contacts, may influence the underlying c-Si surface potential [46, 51, 52]. Consequently, to guarantee high electron selectivity, the Si:H(n) layer of the interband-tunneling contact must be engineered to induce, but also to shield the c-Si surface potential from the presence of the Si:H(p) overlayer.

Requirement III. A final requirement for the thin-film materials used in the tunnel-IBC is dictated by its specific contacting scheme, as shown in Fig. 1e. A low lateral conductance of the Si:H(p) thin film outside the interband-tunneling contact area is mandatory to prevent the electrical connection of the two contact polarities from short-circuiting the device.

To meet **requirement I** of forming an efficient TJ, highly doped n- and p-type Si:H thin-film materials are needed. Current transport mainly occurs by internal field-emission in interband

156 TJs [30] and high doping on both sides of the interface guarantees extremely narrow potential
157 energy barrier widths (see also Fig. 2b), yielding an extremely low contact resistivity.
158 Meanwhile, highly doped Si:H(n) films also help screen the c-Si surface potential from the
159 Si:H(p) overlayer [53] thus preserving good electron selectivity for the interband-tunneling
160 contact (**requirement II**).

161 Highly-crystalline silicon thin films can accommodate a larger number of electrically active
162 dopant atoms, compared to purely amorphous ones, as also evidenced by their higher
163 conductivity (see for instance [54] and Supplementary Table 1). For this, we explored
164 deposition conditions similar to those fostering nanocrystalline silicon thin-film growth [55-57]
165 and silicon epitaxy [58] hence characterized by a considerably lower silane concentration in the
166 deposition plasma than conventional doped a-Si:H layers. Recall that nanocrystalline Si:H thin
167 films typically present a nucleation region where the material is still amorphous, the so-called
168 protocrystalline growth regime [59], which has a thickness that may vary up to several tens of
169 nm, depending on the deposition parameters [60]. In this protocrystalline growth regime, the
170 phase of the growing material also critically depends on the substrate surface chemistry and
171 crystallinity [60]. This substrate selectivity, earlier identified as of prime importance in the
172 technological application of nanocrystalline silicon thin films [61], enables the tunnel-IBC
173 approach.

174 Doped Si:H thin-film materials deposited at low silane concentration were used to fabricate
175 interband-tunneling contacts. The quality of electric transport across such contacts, including
176 the TJ, was evaluated by performing contact resistance measurements. The specific contact

resistivity values for the best TJ materials were measured in the range of 5–10 mΩ cm^2 (see Supplementary Note 1). Note that these values are equal to or lower than those of a variety of state-of-the-art electron passivating contacts, without any embedded TJ [57, 62-67]. Hence, **requirement I** is satisfied using these materials. Additionally, we fabricated two-side-contacted "test" solar cells to evaluate full-area interband-tunneling electron contacts at the back of an otherwise conventional two-side-contacted SHJ solar cell (see Supplementary Note 2). The electrical parameters of these cells are revealing for carrier selectivity and surface passivation properties of the back contact. They showed that our doped Si:H films also satisfy **requirement II**.

Satisfying **requirement III**, demanding low lateral conductance of the Si:H(p) film, contrasts with **requirement I**, to have high material doping and conductivity in the TJ area for efficient transverse carrier transport. We overcame this problem by integrating a sophisticated doped Si:H bilayer into the tunnel-IBC device.

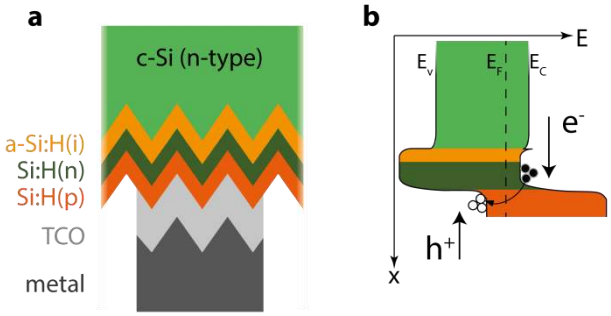

Fig. 2. Interband-tunneling passivating contact for electrons. a, Cross-sectional schematic of the contact composed by a-Si:H(i), and n- and p-type Si:H thin films with the TCO/metal electrode. **b,** Sketch of the electronic band structure with energy levels corresponding to valence band edge (E_V), conduction band edge (E_c) and Fermi level (E_F). Highly doped p- and n-type materials correspond to a narrow depletion region across the TJ, facilitating hole-electron recombination processes.

The key to successful implementation of the tunnel-IBC solar cell

We produced the tunnel-IBC solar cell using a patterned comb of Si:H(n), defined by shadow masking during deposition, as a seed to induce growth of a highly crystalline Si:H(p) material selectively in the area of the TJ. This allowed us to locally achieve a material with high transversal conductivity.

The microstructure of a-Si:H(i)/Si:H(p)/TCO and a-Si:H(i)/Si:H(n)/Si:H(p)/TCO layer stacks deposited onto mirror-polished (111) oriented c-Si wafers was assessed by transmission electron microscopy (TEM). In both types of stacks we find amorphous/crystalline mixed-phase materials. Dark-field scanning TEM (DF STEM) micrographs and inverse Fourier transforms of high-resolution high-angular annular dark-field STEM (HAADF STEM) images highlight the characteristic conical shape of Si crystallites in an amorphous Si matrix [60], with crystals becoming larger along their growth direction (see Fig. 3a, 3b and 3d). A crystallographic analysis by high-resolution HAADF STEM imaging reveals that the Si:H(p) microstructure differs when deposited on a-Si:H(i) (as for the hole contact) compared to when deposited on Si:H(n) (as for the interband-tunneling contact). Indeed, large grains are observed to span across the Si:H(n)/Si:H(p) interface in Fig. 3b, hence indicating that the Si:H(n) layer acts as a nucleation layer for the overlaying Si:H(p) with epitaxy also observed locally across this interface (highlighted by the arrowhead in Fig. 3b and by a higher-magnification view of the interface region in Fig. 3c). In turn, crystals that form during the deposition of the Si:H(p) layer on Si:H(n) quickly grow into crystals with a large cross section (≥10 nm in diameter already at the start of the deposition process). We note that these large grains are also observed by DF STEM imaging

(feature highlighted in Fig. 3a). Additional TEM analysis of the interband-tunneling passivating contact, showing its chemical composition and further evidences of crystalline growth at the Si:H(n)/Si:H(p) interface, are discussed in the supplementary information (Supplementary Note 3). Remarkably, the chemical analysis shown in Supplementary Figure 3 reveals the presence of an oxygen-rich (O-rich) interface between the Si:H(n) and the Si:H(p) layers (as indicated also in Fig. 3c). Alternatively, Si:H(p) grown directly on a-Si:H(i) exhibits characteristic conical shaped crystals that originate from nucleation seeds (see Fig. 3d). Not all of the crystallites appear to grow directly at the interface with the Si:H(i) layer and a thin (≤5 nm) a-Si:H nucleation layer is observed in most regions.

This guarantees a sufficiently low lateral conductance in the Si:H(p) layer and hence a good electrical insulation between the two contact polarities in the tunnel-IBC design. Employing Si:H(p) layers with higher crystallinity and conductivity was found to reduce the shunt resistance and hence to result in lower cell performances, especially at low illumination intensities. Conversely, fully amorphous p-type films did not form efficient TJs - and were found to detrimentally affect the series resistance and the FF of tunnel-IBC solar cells. In Supplementary Note 2, the inadequacy of fully amorphous p-type and n-type films in forming efficient TJ is discussed and demonstrated by means of experiments with two-side contacted SHJ test solar cells.

The difference in growth of amorphous/crystalline mixed-phase silicon materials on c-Si *vs* a-Si:H substrates was earlier discussed according to the cone kinetics model [68, 69]. For the specific substrate, the silicon film morphology can be predicted by a specific “deposition phase

238 diagram" based on growth and nucleation rates of the competing phases [69]. Hence the
239 difference observed in the growth of the Si:H(p) layer on top of the a-Si:H(i) film, when
240 compared to Si:H(n), is expected. When growing on Si:H(n), Si:H(p) grows locally on top of
241 crystalline surfaces, where the "deposition phase diagram" differs from the case of a-Si:H
242 surfaces, resulting in epitaxial growth in some regions. In conclusion, we argue that the
243 inhomogeneous surface conditions at the back, resulting from the alternating a-Si:H(i) and
244 Si:H(n) surfaces, were used to shape in a bottom-up approach two different Si:H(p) thin-film
245 materials, deposited under the same plasma conditions: one formed an efficient TJ and the
246 other formed an efficient hole passivating contact. This was achieved maintaining a sufficiently-
247 low lateral conductance that prevented detrimental short circuits and was facilitated by the
248 protocrystalline growth regime, which is critically surface dependent. Fig. 3d shows a cross-
249 sectional schematic of the resulting doped Si:H bilayer. By this, we resolved the puzzle posed by
250 the conflicting requirements (I and III) and made the patterning of the Si:H(p) layer superfluous.

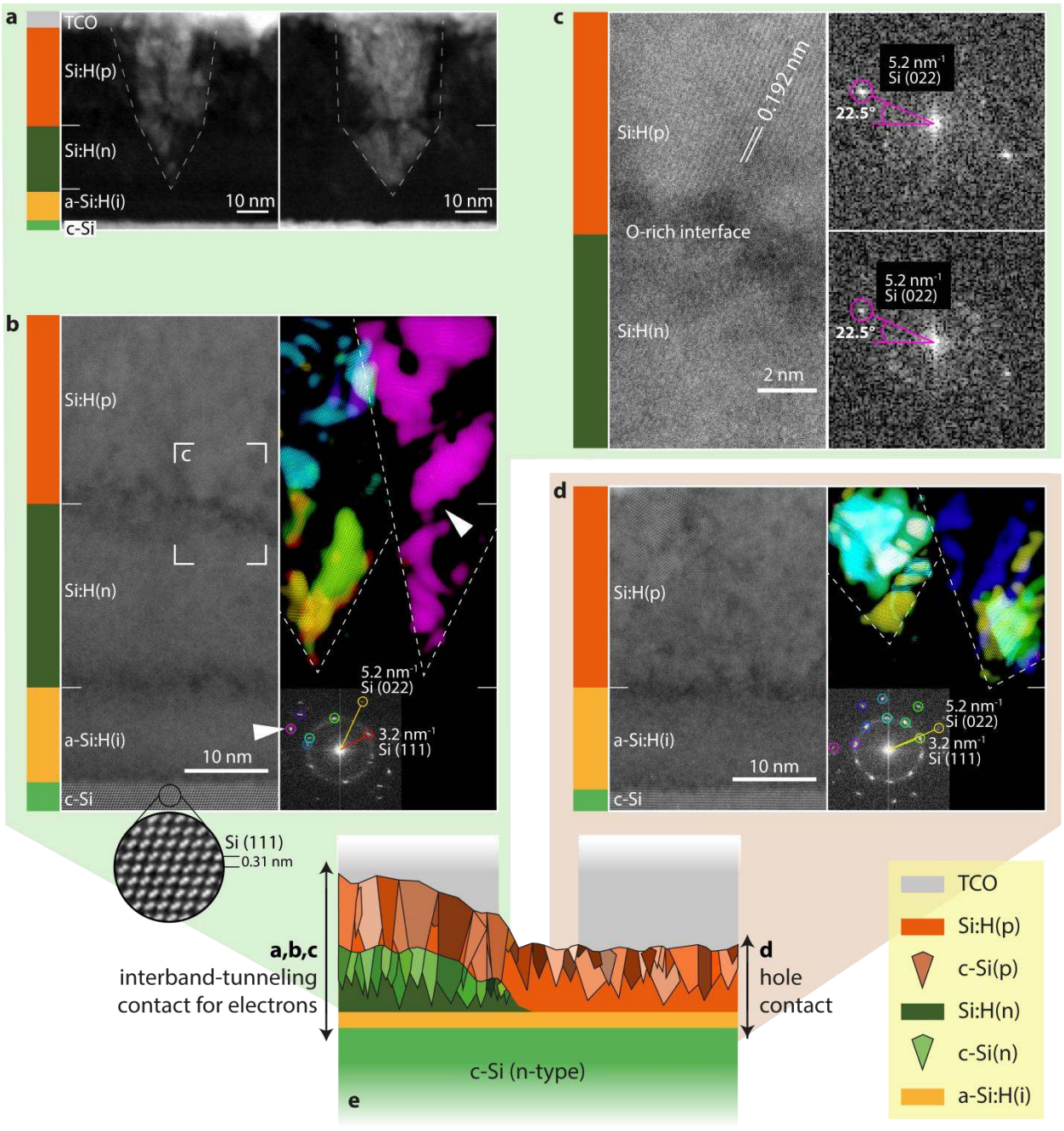

Fig. 3. The doped Si:H bilayer microstructure. a, DF STEM images of the a-Si:H(i)/Si:H(n)/Si:H(p) interband-tunneling passivating contact structure for electrons, highlighting the presence of crystallographic features spanning across the Si:H(n)/Si:H(p) interface. **b,** High-resolution HAADF STEM image of the a-Si:H(i)/Si:H(n)/Si:H(p) structure (left) and corresponding colored inverse Fourier transform of selected symmetric reflections (top right) of the Fourier transform (bottom right, computed excluding the c-Si wafer). We note that in the Fourier transform pattern only one of the symmetric reflections is colored (using the same color as the corresponding inverse Fourier transform) and indexed. The bottom inset shows the Si (111) planes of the wafer viewed along the [011] zone axis. **c,** Higher magnification view of the region highlighted in (c) showing Si (220) planes spanning across the Si:H(n)/SI:H(p) interface, which is oxygen-rich (see Supplementary Note 3). Fourier transforms of the p-type doped (top) and n-type doped (bottom) sides of the interface are shown alongside, demonstrating the epitaxial

relationship between the two layers. **d,** High-resolution HAADF STEM image of the a-Si:H(i)/Si:H(p) hole passivating contact structure (left) and corresponding Fourier transform (bottom right) and colored inverse Fourier transform of selected reflections (top right). **e**, Cross-sectional sketch of the doped Si:H bilayer microstructure in the tunnel-IBC back contact. This special bilayer allows the simultaneous formation of a hole and an electron interband-tunneling contact that are electrically well insulated from each other.

High-efficiency proof-of-concept tunnel-IBC solar cells

Using the Si:H(p) and Si:H(n) thin-film materials examined above, we fabricated tunnel-IBC solar cells with conversion efficiency (η) consistently higher than 22% (see Supplementary Note 4). The highest certified efficiency amounts to 22.6%, with a V_{oc} of 728 mV, for a solar cell featuring a designated area of 9 cm^2. Fig. 4a shows its 1-sun current density-voltage (J-V) characteristic along with the extracted electrical parameters independently confirmed at Fraunhofer ISE CalLab PV Cells testing laboratory (as shown in the Supplementary Note 5). Each device was measured in dark and high reverse-voltage bias up to 30 V with no evidence of breakdown. The shunt-resistance values extracted from these curves were all ≥5 kΩ cm^2, higher than in classical dopant-diffused homojunction c-Si solar cells [70].

After being measured at Fraunhofer ISE, the certified solar cell of Fig. 4a underwent light-soaking for 30 h at 1-sun irradiance. After light soaking, following the procedure described in the Methods section, we measured in-house the electrical parameters, and the J-V characteristic, reported in Fig. 4b. Light-soaking improved the conversion efficiency by about 0.3% absolute, in agreement with the recent findings of Kobayashi *et al.* [31]. With this measurement, we demonstrated a maximum conversion efficiency of 22.9% for the tunnel-IBC solar cell.

The conversion efficiency level of these demonstrator devices was achieved by using a more transparent front side stack [15] compared to our earlier back-contacted devices [36], enhancing the J_{sc} of the cell. Also, widening the TCO/metal fingers of the hole contact to exploit the homogenously-thick Si:H(p) layer improved carrier collection [35]. These adjustments in

289 combination with the designed material properties of the doped Si:H bilayer all contributed to
290 the improved efficiency.

291 Next steps to achieve higher efficiencies can be based on using thinner c-Si wafers to increase
292 the open-circuit voltage of the solar cell, combined with improved light-management schemes
293 to increase its short-circuit density. At the front, the replacement of the a-Si:H(i) film with a
294 highly-transparent dielectric passivating layer can decrease parasitic absorption of short-
295 wavelength photons. Alternatively, the use of a sub-nm a-Si:H film capped by SiN_x [71] looks
296 also an interesting and simple option. At the rear, the integration of advanced reflectors into
297 our contacts can improve the red response of the cell [72]. Finally, the reduction of the device
298 series resistance and the improvement in passivation quality at the maximum power point, as
299 recently pointed out by Adachi *et al*. [73], are required to achieve higher FF values. A more
300 detailed discussion of the efficiency losses affecting this best tunnel-IBC, compared to the
301 record device fabricated by Kaneka [26] using the conventional IBC-SHJ architecture, is reported
302 in the Supplementary Note 4.

303 We underline that our device concept may also be suitable for other materials used in
304 passivating contacts, such as transition metal oxide or alkali earth metal and alkali metal
305 fluoride materials [62-64, 74]. We recall an earlier work where a TiO_x thin film, interposed
306 between p- and n-type a-Si:H films connecting two sub-cells of a tandem thin-film device, was
307 found to be beneficial for the performance of the solar cell [75]. This would extend further the
308 scope of this work and make the tunnel-IBC the approach of choice for designing the
309 architecture of back-contacted devices with passivating contacts.

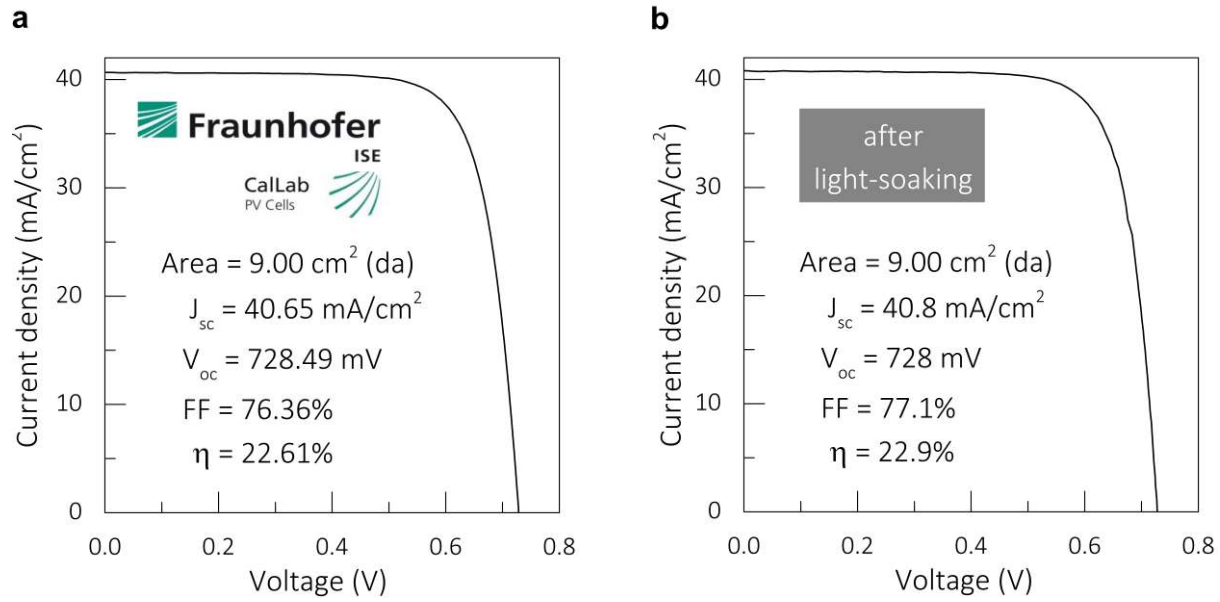

Fig. 4. Best tunnel-IBC solar cell. a, 1 sun J-V characteristic of the most efficient tunnel-IBC device independently confirmed at Fraunhofer ISE CalLab PV Cell testing laboratory (as shown in the Supplementary Note 5). The solar cell shows an outstanding conversion efficiency (η >22.5%) with a simple back-contacted structure and fabrication process. **b,** In-house measured 1-sun J-V characteristic of the certified tunnel-IBC in (**a**) after light-soaking for 30 h at 1-sun irradiance, resulting in a conversion efficiency of 22.9%.

Conclusions

In this work we demonstrated a novel low-temperature interdigitated back-contacted c-Si solar cell with passivating contacts and high efficiency, where patterning and alignment complexity are significantly minimized: the tunnel-IBC.

Key to the success of this solar cell is a special bilayer of doped hydrogenated silicon thin films, with a functionalized microstructure: highly-crystalline or partly amorphous, where high doping or low lateral conductance is respectively needed. We achieved these unique properties by selecting a protocrystalline growth regime, where the microstructure of the growing material is defined by the substrate surface. This special film is used to simultaneously form an effective interband-tunneling passivating contact for electrons and a hole passivating contact that are electrically well-insulated from each other.

Proof-of-concept devices with high conversion efficiency over 22.5% have been achieved with excellent V_{oc} of about 730 mV and J_{sc} always surpassing abundantly the 40 mA/cm^2. These results are among the best reported for solar cells with SHJ contacts based on traditional IBC schemes.

The combination of back-contacted and passivating contact technologies defines the ultimate c-Si single-junction solar cell architecture. However, its practical implementation has remained challenging, especially with respect to industrially viable processes. The tunnel-IBC concept contributes to solve this problem delineating a realistic approach with little fabrication complexity and an entire new class of back-contacted solar cells.

Methods

Solar cell fabrication and characterization. Tunnel-IBC devices were fabricated on n-type, 250-µm-thick 4-inch float-zone (100) oriented c-Si wafers with a nominal resistivity of 3 Ω cm. The device has an active area of 9 cm^2, excluding the bus bar region, and was placed at the center of the wafer. Wafers were textured in a potassium hydroxide solution, forming pyramids of 5 to 10 µm in size featuring (111) c-Si oriented facets, and cleaned by a wet-chemical process. Following a short dip in a diluted hydrofluoric solution, a thin a-Si:H(i) film of about 6 nm was deposited on both entire wafer surfaces as a passivating layer. Doped Si:H materials, deposited at higher hydrogen-to-silane gas-flow ratios, were used as a hole-collecting layer as well as to form the interband-tunneling passivating contact for electrons. Intrinsic a-Si:H and doped Si:H layers were grown at temperatures ≤ 200 °C by means of PECVD in Octopus II and Octopus I reactors from INDEOtec SA, respectively. The front side SiN_x ARC was deposited by PECVD at a low temperature (200 °C). A full-area TCO/metal stack consisting of a sputtered TCO and Ag was used to fabricate the back contact. Patterning of the interdigitated back electrodes was achieved by hot-melt inkjet printing of an etch resist with the commercial system PiXDRO LP50 of Meyer Burger (Netherlands) B. V. and subsequent wet-chemical etching in an acidic solution [36]. After wet-chemical etching, the inkjet-printed etch resist was removed using a liquid solvent. Before solar cell characterization, a curing process at about 200 °C in a belt furnace was carried out to repair a-Si:H(i) and doped Si:H layers from potentially present sputter-induced damage [76].

The light J-V characteristic of the solar cell shown in Fig. 4a was measured at the Fraunhofer ISE CalLab PV Cells testing laboratory, Freiburg, Germany. This certified solar cell was used to calibrate a second tunnel-IBC solar cell that we used as reference for the in-house J-V measurements shown in Fig. 4b and in the Supplementary Table 3 and 4. These in-house measurements were performed under standard test conditions (AM 1.5G spectrum, 100 mW cm^{-2}, 25 °C), with a Wacom WXS-90S-L2 solar simulator and

without applying spectral mismatch correction. A black-anodized aluminium mask was used while measuring in order to define the solar cell designated area. Shunt-resistance values were extracted from the slope of a linear fit to the dark J-V characteristic in the range (0,-100) mV.

Material characterization. For TEM observations, a-Si:H(i)/Si:H(p)/TCO and a-Si:H(i)/Si:H(n)/Si:H(p)/TCO layer stacks were deposited onto mirror-polished (111) oriented c-Si wafers . Such surface orientation was chosen as pyramidally textured (100) oriented c-Si wafers used for tunnel-IBC device fabrication feature (111) oriented facets. Thin cross sections were prepared using the conventional focused ion-beam lift-out method in a Zeiss NVision 40 using a final milling voltage of 2 kV to reduce Ga-induced surface damage. STEM DF images were recorded in an FEI Tecnai Osiris microscope, while high-resolution HAADF micrographs were obtained in an image and probe Cs corrected FEI Titan Themis microscope. Both systems were operated at 200 kV with a beam current of about 100 pA. For HAADF imaging, the beam convergence semi-angle was set to 28 mrad and the camera length to 115 mm (corresponding to an HAADF detector collection semi-angle of 55.5 to 200 mrad). Inverse Fourier transforms of high-resolution HAADF images were computed using a homemade Mathematica script [77], with a mask diameter of 0.8 nm^{-1} centered on selected reflections. Contrast, brightness and gamma values of inverse Fourier transform images were adjusted to highlight the crystallites of interest. Additional TEM experiments, performed using the FEI Titan Themis microscope, are discussed in Supplementary Note 3 and include high-resolution TEM imaging and energy-dispersive X-ray (EDX) spectroscopy mapping. EDX maps were recorded with a beam current of 200 pA and a solid angle >0.7 srad, using four quadrant silicon drift detectors (see Supplementary Figure 3).

References

[1] A. Jäger-Waldau, "PV Status Report 2016," *JRC Science for Policy Report*, 2016.

[2] C. Battaglia, A. Cuevas, and S. De Wolf, "High-efficiency crystalline silicon solar cells: status and perspectives," *Energy & Environmental Science*, vol. 9, no. 5, pp. 1552-1576, 2016.

[3] International Energy Agency, "Snapshot of Global Photovoltaic Markets," *Photovoltaic Power System Programme (PVPS), Technical report*, 2016.

[4] D. M. Powell, M. T. Winkler, H. J. Choi, C. B. Simmons, D. B. Needleman, and T. Buonassisi, "Crystalline silicon photovoltaics: a cost analysis framework for determining technology pathways to reach baseload electricity costs," *Energy & Environmental Science*, vol. 5, no. 3, pp. 5874-5883, 2012.

[5] M. A. Green, "Commercial progress and challenges for photovoltaics," *Nature Energy*, vol. 1, pp. 15015, 2016.

[6] S. W. Glunz, F. Feldmann, A. Richter, M. Bivour, C. Reichel, H. Steinkemper, J. Benick, and M. Hermle, "The irresistible charm of a simple current flow pattern - 25% with a solar cell featuring a full-area back contact," in *Proc. 31st Eur. Photovoltaic Sol. Energy Conf. Exhib.*, Hamburg, Germany, 2015

[7] D. Adachi, J. L. Hernández, and K. Yamamoto, "Impact of carrier recombination on fill factor for large area heterojunction crystalline silicon solar cell with 25.1% efficiency," *Applied Physics Letters*, vol. 107, no. 23, pp. 233506, 2015.

[8] M. Aleman, J. Das, T. Janssens, B. Pawlak, N. Posthuma, J. Robbelein, S. Singh, K. Baert, J. Poortmans, J. Fernandez, K. Yoshikawa, and P. J. Verlinden, "Development and Integration of a High Efficiency Baseline Leading to 23% IBC Cells," *Energy Procedia*, vol. 27, pp. 638-645, 2012.

[9] R. Peibst, N.-P. Harder, A. Merkle, T. Neubert, S. Kirstein, J. Schmidt, F. Dross, P.A. Basore, and R. Brendel, "High-Efficiency RISE-IBC Solar Cells: Influence of Rear Side-Passivation on pn-Junction Meander Recombination," in *Proc. 28th European Photovoltaic Solar Energy Conference and Exhibition* Paris, France, 2013, pp. 971-975.

[10] C. Reichel, F. Granek, M. Hermle, and S. W. Glunz, "Back-contacted back-junction n-type silicon solar cells featuring an insulating thin film for decoupling charge carrier collection and metallization geometry," *Progress in Photovoltaics: Research and Applications*, vol. 21, no. 5, pp. 1063-1076, 2013.

[11] H. Savin, P. Repo, G. Von Gastrow, P. Ortega, E. Calle, M. Garín, and R. Alcubilla, "Black silicon solar cells with interdigitated back-contacts achieve 22.1% efficiency," *Nat Nano*, vol. 10, no. 7, pp. 624-628, 2015.

[12] E. Franklin, K. Fong, K. Mcintosh, A. Fell, A. Blakers, T. Kho, D. Walter, D. Wang, N. Zin, M. Stocks, E.-C. Wang, N. Grant, Y. Wan, Y. Yang, X. Zhang, Z. Feng, and P. J. Verlinden, "Design, fabrication and characterisation of a 24.4% efficient interdigitated back contact solar cell," *Progress in Photovoltaics: Research and Applications*, vol. 24, no. 4, pp. 411-427, 2016.

[13] M. A. Green, K. Emery, Y. Hishikawa, W. Warta, and E. D. Dunlop, "Solar cell efficiency tables (version 48)," *Progress in Photovoltaics: Research and Applications*, vol. 24, no. 7, pp. 905-913, 2016.

[14] S.-Y. Lee, H. Choi, H. Li, K. Ji, S. Nam, J. Choi, S.-W. Ahn, H.-M. Lee, and B. Park, "Analysis of a-Si:H/TCO contact resistance for the Si heterojunction back-contact solar cell," *Solar Energy Materials and Solar Cells*, vol. 120, Part A, pp. 412-416, 2014.

[15] B. Paviet-Salomon, A. Tomasi, A. Descoeudres, L. Barraud, S. Nicolay, M. Despeisse, S. De Wolf, and C. Ballif, "Back-Contacted Silicon Heterojunction Solar Cells: Optical-Loss Analysis and Mitigation," *Photovoltaics, IEEE Journal of*, vol. 5, no. 5, pp. 1293-1303, 2015.

[16] M. Xu, T. Bearda, H. Sivaramakrishnan Radhakrishnan, S. Kiran Jonnak, M. Filipic, V. Depauw, K. Van Nieuwenhuysen, Y. Abdulraheem, M. Debucquoy, I. Gordon, J. Szlufcik, and J. Poortmans, "Process Development of Silicon Heterojunction Interdigitated Back-Contacted (SHJ-IBC) Solar Cells Bonded to Glass," in *Proc. 32nd European Photovoltaic Solar Energy Conference and Exhibition (EUPVSEC)*, Munich, Germany, 2016

[17] O. N. Aguila, S. Harrison, and G. D'alonzo, "Laser ablation process for patterning back-contact heterojunction cells," in *Proc. 7th Workshop on Back Contact Solar Cell and Module Technology*, Freiburg, Germany, 2015

[18] N. Mingirulli, J. Haschke, R. Gogolin, R. Ferre, T. F. Schulze, J. Dusterhoft, N. P. Harder, L. Korte, R. Brendel, and B. Rech, "Efficient interdigitated back-contacted silicon heterojunction solar cells," *Phys. Status Solidi-Rapid Res. Lett.*, vol. 5, no. 4, pp. 159-161, 2011.

[19] L. Zhang, U. K. Das, Z. Shu, H. Liu, R. W. Birkmire, and S. S. Hegedus, "Experimental and simulated analysis of p a-Si:H defects on silicon heterojunction solar cells: trade-offs between Voc and FF," in *Proc. 42nd IEEE Photovoltaic Specialist Conference (PVSC)*, 2015, pp. 1-5.

[20] G. Yang, A. Ingenito, O. Isabella, and M. Zeman, "IBC c-Si solar cells based on ion-implanted poly-silicon passivating contacts," *Solar Energy Materials and Solar Cells*, vol. 158, Part 1, pp. 84-90, 2016.

[21] M. Rienäcker, M. Bossmeyer, A. Merkle, U. Römer, F. Haase, J. Krügener, R. Brendel, and R. Peibst, "Junction Resistivity of Carrier-Selective Polysilicon on Oxide Junctions and Its Impact on Solar Cell Performance," *IEEE Journal of Photovoltaics*, vol. 7, no. 1, pp. 11-18, 2017.

[22] F. Haase, F. Kiefer, J. Krügener, R. Brendel, and R. Peibst, "IBC solar cells with polycrystalline on oxide (POLO) passivating contacts for both polarities," in *Proc. 26th Photovoltaic Science and Engineering Conference (PVSEC)*, Singapore, 2016

[23] D. D. Smith, P. Cousins, S. Westerberg, R. De Jesus-Tabajonda, G. Aniero, and S. Yu-Chen, "Toward the Practical Limits of Silicon Solar Cells," *Photovoltaics, IEEE Journal of*, vol. 4, no. 6, pp. 1465-1469, 2014.

[24] K. Masuko, M. Shigematsu, T. Hashiguchi, D. Fujishima, M. Kai, N. Yoshimura, T. Yamaguchi, Y. Ichihashi, T. Mishima, N. Matsubara, T. Yamanishi, T. Takahama, M. Taguchi, E. Maruyama, and S. Okamoto, "Achievement of More Than 25% Conversion Efficiency With Crystalline Silicon Heterojunction Solar Cell," *Photovoltaics, IEEE Journal of*, vol. 4, no. 6, pp. 1433-1435, 2014.

[25] J. Nakamura, N. Asano, T. Hieda, C. Okamoto, H. Katayama, and K. Nakamura, "Development of Heterojunction Back Contact Si Solar Cells," *Photovoltaics, IEEE Journal of*, vol. 4, no. 6, pp. 1491-1495, 2014.

[26] *World's Highest Conversion Efficiency of 26.33% Achieved in a Crystalline Silicon Solar Cell*. News Release, Kaneka Corporation Public Relations Office and New Energy and Industrial Technology Development Organization (NEDO), http://www.kaneka.co.jp/kaneka-e/images/topics/1473811995/1473811995_101.pdf, Sep. 2016.

[27] S. De Wolf, A. Descoeudres, Z. C. Holman, and C. Ballif, "High-efficiency Silicon Heterojunction Solar Cells: A Review," *Green*, vol. 2, pp. 7-24, 2012.

[28] National Renewable Energy Laboratory (NREL) Efficiency Chart, http://www.nrel.gov/pv/assets/images/efficiency_chart.jpg, December 2016.

[29] A. Richter, M. Hermle, and S. W. Glunz, "Reassessment of the Limiting Efficiency for Crystalline Silicon Solar Cells," *IEEE Journal of Photovoltaics*, vol. 3, no. 4, pp. 1184-1191, 2013.

[30] L. Esaki, "New Phenomenon in Narrow Germanium *p-n* Junctions," *Physical Review*, vol. 109, pp. 603-604, 1958.

[31] E. Kobayashi, S. De Wolf, J. Levrat, G. Christmann, A. Descoeudres, S. Nicolay, M. Despeisse, Y. Watabe, and C. Ballif, "Light-induced performance increase of silicon heterojunction solar cells," *Applied Physics Letters*, vol. 109, no. 15, pp. 153503, 2016.

[32] D. A. Spee, "Preparations for Making Back Contacted Heterojunction Solar Cells," *Master Thesis*, 2008.

[33] S. Y. Herasimenka, C. J. Tracy, W. J. Dauksher, C. B. Honsberg, and S. Bowden, "A simplified process flow for silicon heterojunction interdigitated back contact solar cells: Using shadow masks and tunnel junctions," in *Proc. 2014 IEEE 40th Photovoltaic Specialist Conference (PVSC)*, 2014, pp. 2486-2490.

[34] M. Lu, S. Bowden, U. Das, and R. Birkmire, "Interdigitated back contact silicon heterojunction solar cell and the effect of front surface passivation," *Applied Physics Letters*, vol. 91, no. 6, pp. 063507, 2007.

[35] M. Hermle, F. Granek, O. Schultz-Wittmann, and S. W. Glunz, "Shading effects in back-junction back-contacted silicon solar cells," in *Proc. 33rd IEEE Photovoltaic Specialists Conference (PVSC)*, St. Diego, CA, USA, 2008, pp. 1-4.

[36] A. Tomasi, B. Paviet-Salomon, D. Lachenal, S. M. De Nicolas, A. Descoeudres, J. Geissbuhler, S. De Wolf, and C. Ballif, "Back-Contacted Silicon Heterojunction Solar Cells With Efficiency >21% " *Photovoltaics, IEEE Journal of*, vol. 4, no. 4, pp. 1046-1054, 2014.

[37] C. Amano, H. Sugiura, A. Yamamoto, and M. Yamaguchi, "20.2% efficiency $Al_{0.4}Ga_{0.6}As$/GaAs tandem solar cells grown by molecular beam epitaxy," *Applied Physics Letters*, vol. 51, no. 24, pp. 1998-2000, 1987.

[38] J. Meier, S. Dubail, D. Fischer, J. a. A. Selvan, N. P. Vaucher, R. Platz, C. Hof, R. Flückiger, U. Kroll, N. Wyrsch, P. Torres, H. Keppner, A. Shah, and K.-D. Ufert, "The 'Micromorph' Solar Cells: a New Way to High Efficiency Thin Film Silicon Solar Cells," *Proceedings of the 13th EC Photovoltaic Solar Energy Conference*, vol., pp. 1445–1450, 1995.

[39] J.-W. Schüttauf, B. Niesen, L. Löfgren, M. Bonnet-Eymard, M. Stuckelberger, S. Hänni, M. Boccard, G. Bugnon, M. Despeisse, F.-J. Haug, F. Meillaud, and C. Ballif, "Amorphous silicon–germanium for triple and quadruple junction thin-film silicon based solar cells," *Solar Energy Materials and Solar Cells*, vol. 133, pp. 163-169, 2015.

[40] S. Essig, J. Benick, M. Schachtner, A. Wekkeli, M. Hermle, and F. Dimroth, "Wafer-Bonded GaInP/GaAs//Si Solar Cells With 30% Efficiency Under Concentrated Sunlight," *IEEE Journal of Photovoltaics*, vol. 5, no. 3, pp. 977-981, 2015.

[41] J. P. Mailoa, C. D. Bailie, E. C. Johlin, E. T. Hoke, A. J. Akey, W. H. Nguyen, M. D. Mcgehee, and T. Buonassisi, "A 2-terminal perovskite/silicon multijunction solar cell enabled by a silicon tunnel junction," *Applied Physics Letters*, vol. 106, no. 12, pp. 121105, 2015.

[42] J. Werner, C.-H. Weng, A. Walter, L. Fesquet, J. P. Seif, S. De Wolf, B. Niesen, and C. Ballif, "Efficient Monolithic Perovskite/Silicon Tandem Solar Cell with Cell Area >1 cm^2," *The Journal of Physical Chemistry Letters*, vol. 7, no. 1, pp. 161-166, 2016.

[43] H. Fujiwara and M. Kondo, "Effects of a-Si:H layer thicknesses on the performance of a-Si:H/c-Si heterojunction solar cells," *Journal of Applied Physics*, vol. 101, no. 5, pp. 054516, 2007.

[44] A. Kanevce and W. K. Metzger, "The role of amorphous silicon and tunneling in heterojunction with intrinsic thin layer (HIT) solar cells," *Journal of Applied Physics*, vol. 105, no. 9, pp. 094507, 2009.

[45] A. Tomasi, "Back-contacted silicon heterojunction solar cells," *Ph.D. Dissertation*, 2016.

[46] A. Tomasi, F. Sahli, J. P. Seif, L. Fanni, S. M. De Nicolas Agut, J. Geissbuhler, B. Paviet-Salomon, S. Nicolay, L. Barraud, B. Niesen, S. De Wolf, and C. Ballif, "Transparent Electrodes in Silicon Heterojunction Solar Cells: Influence on Contact Passivation," *Photovoltaics, IEEE Journal of*, vol. 6, no. 1, pp. 17-27, 2016.

[47] A. Tomasi, B. Paviet-Salomon, D. Lachenal, S. Martin De Nicolas, M. Ledinsky, A. Descoeudres, S. Nicolay, S. De Wolf, and C. Ballif, "Photolithography-free interdigitated back-contacted silicon heterojunction solar cells with efficiency >21%," in *Proc. 40th IEEE Photovoltaic Specialist Conference (PVSC)*, 2014, pp. 3644-3648.

[48] M. Ledinský, B. Paviet-Salomon, A. Vetushka, J. Geissbühler, A. Tomasi, M. Despeisse, S. De Wolf , C. Ballif , and A. Fejfar, "Profilometry of thin films on rough substrates by Raman spectroscopy," *Scientific Reports*, vol. 6, pp. 37859, 2016.

[49] U. Wurfel, A. Cuevas, and P. Wurfel, "Charge Carrier Separation in Solar Cells," *Photovoltaics, IEEE Journal of*, vol. 5, no. 1, pp. 461-469, 2015.

[50] R. Brendel and R. Peibst, "Contact Selectivity and Efficiency in Crystalline Silicon Photovoltaics," *IEEE Journal of Photovoltaics*, vol. 6, no. 6, pp. 1413-1420, 2016.

[51] R. Rößler, C. Leendertz, L. Korte, N. Mingirulli, and B. Rech, "Impact of the transparent conductive oxide work function on injection-dependent a-Si:H/c-Si band bending and solar cell parameters," *Journal of Applied Physics*, vol. 113, no. 14, pp. 144513, 2013.

[52] B. Macco, D. Deligiannis, S. Smit, R. a. C. M. M. V. Swaaij, M. Zeman, and W. M. M. Kessels, "Influence of transparent conductive oxides on passivation of a-Si:H/c-Si heterojunctions as studied by atomic layer deposited Al-doped ZnO," *Semiconductor Science and Technology*, vol. 29, no. 12, pp. 122001, 2014.

[53] S. M. Sze and K. K. Ng, *Physics of Semiconductor Devices*, 3rd ed. 2006, John Wiley & Sons.

[54] P. Alpuim, V. Chu, and J. P. Conde, "Doping of amorphous and microcrystalline silicon films deposited at low substrate temperatures by hot-wire chemical vapor deposition," *Journal of Vacuum Science & Technology A*, vol. 19, no. 5, pp. 2328-2334, 2001.

[55] B. Strahm, A. A. Howling, L. Sansonnens, and H. Ch, "Plasma silane concentration as a determining factor for the transition from amorphous to microcrystalline silicon in SiH_4/H_2 discharges," *Plasma Sources Science and Technology*, vol. 16, no. 1, pp. 80, 2007.

[56] J. P. Seif, A. Descoeudres, G. Nogay, S. Hanni, S. Martin De Nicolas, N. Holm, J. Geissbuhler, A. Hessler-Wyser, M. Duchamp, R. E. Dunin-Borkowski, M. Ledinsky, S. De Wolf, and C. Ballif, "Strategies for Doped Nanocrystalline Silicon Integration in Silicon Heterojunction Solar Cells," *IEEE Journal of Photovoltaics*, vol. 6, no. 5, pp. 1132-1140, 2016.

[57] G. Nogay, J. P. Seif, Y. Riesen, A. Tomasi, Q. Jeangros, N. Wyrsch, F. J. Haug, S. D. Wolf, and C. Ballif, "Nanocrystalline Silicon Carrier Collectors for Silicon Heterojunction Solar Cells and Impact on Low-Temperature Device Characteristics," *IEEE Journal of Photovoltaics*, vol. 6, no. 6, pp. 1654-1662, 2016.

[58] B. Demaurex, R. Bartlome, J. P. Seif, J. Geissbühler, D. T. L. Alexander, Q. Jeangros, C. Ballif, and S. De Wolf, "Low-temperature plasma-deposited silicon epitaxial films: Growth and properties," *Journal of Applied Physics*, vol. 116, no. 5, 2014.

[59] J. Koh, Y. Lee, H. Fujiwara, C. R. Wronski, and R. W. Collins, "Optimization of hydrogenated amorphous silicon p–i–n solar cells with two-step i layers guided by real-time spectroscopic ellipsometry," *Applied Physics Letters*, vol. 73, no. 11, pp. 1526-1528, 1998.

[60] R. W. Collins, A. S. Ferlauto, G. M. Ferreira, C. Chen, J. Koh, R. J. Koval, Y. Lee, J. M. Pearce, and C. R. Wronski, "Evolution of microstructure and phase in amorphous, protocrystalline, and microcrystalline silicon studied by real time spectroscopic ellipsometry," *Solar Energy Materials and Solar Cells*, vol. 78, no. 1–4, pp. 143-180, 2003.

[61] P. R. I. Cabarrocas, N. Layadi, T. Heitz, B. Drévillon, and I. Solomon, "Substrate selectivity in the formation of microcrystalline silicon: Mechanisms and technological consequences," *Applied Physics Letters*, vol. 66, no. 26, pp. 3609-3611, 1995.

[62] J. Bullock, M. Hettick, J. Geissbühler, A. J. Ong, T. Allen, Carolin m. Sutter Fella, T. Chen, H. Ota, E. W. Schaler, S. De Wolf, C. Ballif, A. Cuevas, and A. Javey, "Efficient silicon solar cells with dopant-free asymmetric heterocontacts," *Nature Energy*, vol. 1, pp. 15031, 2016.

[63] X. Yang, Q. Bi, H. Ali, K. Davis, W. V. Schoenfeld, and K. Weber, "High-Performance TiO2-Based Electron-Selective Contacts for Crystalline Silicon Solar Cells," *Advanced materials*, vol. 28, no. 28, pp. 5891-5897, 2016.

[64] Y. Wan, C. Samundsett, J. Bullock, T. Allen, M. Hettick, D. Yan, P. Zheng, X. Zhang, J. Cui, J. Mckeon, A. Javey, and A. Cuevas, "Magnesium Fluoride Electron-Selective Contacts for Crystalline Silicon Solar Cells," *ACS Applied Materials & Interfaces*, vol. 8, no. 23, pp. 14671-14677, 2016.

[65] R. Gogolin, M. Turcu, R. Ferre, J. Clemens, N. P. Harder, R. Brendel, and J. Schmidt, "Analysis of Series Resistance Losses in a-Si:H/c-Si Heterojunction Solar Cells," *Photovoltaics, IEEE Journal of*, vol. 4, no. 5, pp. 1169-1176, 2014.

[66] W. Tatsuro, F. Takeo, M. Tsutomu, S. Tomohiro, S. Yusuke, M. Takayuki, H. Tetsuro, Y. Yohei, K. Shintaro, S. Yuichi, T. Hidetada, K. Yoshihiko, and F. Hiroyuki, "Rear-emitter Si heterojunction solar cells with over 23% efficiency," *Applied Physics Express*, vol. 8, no. 2, pp. 021402, 2015.

[67] U. Römer, R. Peibst, T. Ohrdes, B. Lim, J. Krügener, E. Bugiel, T. Wietler, and R. Brendel, "Recombination behavior and contact resistance of n+ and p+ poly-crystalline Si/mono-crystalline Si junctions," *Solar Energy Materials and Solar Cells*, vol. 131, pp. 85-91, 2014.

[68] C. W. Teplin, E. Iwaniczko, B. To, H. Moutinho, P. Stradins, and H. M. Branz, "Breakdown physics of low-temperature silicon epitaxy grown from silane radicals," *Physical Review B*, vol. 74, no. 23, pp. 235428, 2006.

[69] C. W. Teplin, C.-S. Jiang, P. Stradins, and H. M. Branz, "Cone kinetics model for two-phase film silicon deposition," *Applied Physics Letters*, vol. 92, no. 9, pp. 093114, 2008.

[70] A. Khanna, T. Mueller, R. A. Stangl, B. Hoex, P. K. Basu, and A. G. Aberle, "A Fill Factor Loss Analysis Method for Silicon Wafer Solar Cells," *IEEE J. Photovoltaics*, vol. 3, no. 4, pp. 1170-1177, 2013.

[71] Y. Wan, D. Yan, J. Bullock, X. Zhang, and A. Cuevas, "Passivation of c-Si surfaces by sub-nm amorphous silicon capped with silicon nitride," *Applied Physics Letters*, vol. 107, no. 23, pp. 231606, 2015.

[72] Z. C. Holman, A. Descoeudres, S. De Wolf, and C. Ballif, "Record Infrared Internal Quantum Efficiency in Silicon Heterojunction Solar Cells With Dielectric/Metal Rear Reflectors," *IEEE J. Photovoltaics*, vol. 3, no. 4, pp. 1243-1249, 2013.

[73] D. Adachi, J. L. Hernández, and K. Yamamoto, "Impact of carrier recombination on fill factor for large area heterojunction crystalline silicon solar cell with 25.1% efficiency," *Applied Physics Letters*, vol. 107, no. 23, pp. 233506, Dec. 2015.

[74] J. Geissbühler, J. Werner, S. M. De Nicolas, L. Barraud, A. Hessler-Wyser, M. Despeisse, S. Nicolay, A. Tomasi, B. Niesen, S. De Wolf, and C. Ballif, "22.5% efficient silicon heterojunction solar cell with molybdenum oxide hole collector," *Applied Physics Letters*, vol. 107, no. 8, pp. 081601, 2015.

[75] Y. Sakai, K. Fukuyama, M. Matsumura, Y. Nakato, and H. Tsubomura, "The effect of interposing thin oxide layers on the photovoltaic properties of a-Si:H solar cells II between the middle n and p layers of a tandem-type cell," *Journal of Applied Physics*, vol. 64, no. 1, pp. 394-398, 1988.

606 [76] B. Demaurex, S. De Wolf, A. Descoeudres, Z. Charles Holman, and C. Ballif, "Damage at
607 hydrogenated amorphous/crystalline silicon interfaces by indium tin oxide overlayer
608 sputtering," *Applied Physics Letters*, vol. 101, no. 17, pp. 171604, 2012.

609 [77] Wolfram Research, "Mathematica," Champaign, Illinois, 2016.

610

611

Acknowledgements

This work was supported by the Swiss Commission for Technology and Innovation (CTI) by the Swiss Federal Office for Energy (SFOE), and by the Fonds National Suisse Reequip Program. The authors thank Meyer Burger Research for scientific partnership and financial support; D. Lachenal and B. Strahm for support and collaboration in back-contacted silicon heterojunction solar cell development; J. Hermans and Meyer Burger B.V. for the support in inkjet printing; M. Pickrell and SunChemicals for supplying the hot melt; the Academic Writing Services at KAUST for text editing; M. J. Lehmann, N. Badel and H. Watanabe at EPFL&CSEM for their support in back-end processing; and A. Hessler at EPFL and CIME for the TEM observations.

Author contributions

A.T., B.P.-S., M.D. and C.B. conceived the idea. A.T. designed the experiments and carried out the device fabrication in collaboration with B.P.-S.. Q.J. carried out the TEM observations. L.B. and A.D. developed the a-Si:H(i) passivating films. J.P.S. contributed to the development of the doped Si:H thin-film materials. S.N. and G.C. developed and deposited the TCO material. J.H. and S.D.W. contributed to the definition and presentation of the paper contents. S.D.W., M.D. and C.B. discussed the results and organized the research. A.T. wrote the paper, and all other authors provided feedback.